ISBN: 978-3-95450-184-7 doi:10.18429/JACoW-IPAC2018-THPAF080

SIS100 BEAM DYNAMICS CHALLENGES RELATED TO THE MAGNET SYSTEM

V. Kornilov, V. Chetvertkova, S. Sorge, P. J. Spiller,
GSI Helmholtzzentrum, Darmstadt, Germany
O. Boine-Frankenheim, GSI Helmholtzzentrum and TU Darmstadt, Germany

INTRODUCTION

The SIS100 synchrotron [1] is the central accelerator of the upcoming FAIR project [2] at GSI, Darmstadt, Germany. The major challenges of the future operation are related to high-intensity, low beam loss operation for a wide range of ion species and charge states, for different operational cycles and extraction schemes. The magnet system [3] consists of 108 dipole, 166 quadrupole and additional correction magnets. The magnets are presently under production and testing, with detailed measurements of the magnetic field imperfections. This results will eventually construct the complete database for the SIS100 magnet system.

The delivery of the series dipole magnets to GSI is presently in progress [4]. In this paper, we analyze the magnetic filed data for the four series dipole magnets. The implications of the magnetic field imperfections for the single-particle stability are studied.

FIELD ERRORS IN DIPOLE MAGNETS

The SIS100 dipole magnets [3, 4] are superferric superconducting magnets. The iron yoke is bent, the length is 3 m and the curvature radius is $\rho = 52.632$ m. A magnet testing facility with a rotating coil system [5] has been established at GSI Darmstadt. The coil length is 600 mm, the shaft covers the full magnet by 5 segments, the coil radius is 14.53 mm. Longitudinal positions of the measurement coil for the magnet sides are ±1400 mm. The results for the magnet body (the central part) are given by measurements at three positions along the magnet: at the center and at ±700 mm.

The magnetic field representation using the harmonic coefficients B_n, A_n is

$$B_y + iB_x = (B_n + iA_n)\left(\frac{x+iy}{r_0}\right)^{n-1}, \qquad (1)$$

where the reference radius is $r_0 = 30$ mm in our case. B_n are the normal components, A_n are the skew components. B_1 is the dipole, B_2 is the quadrupole, etc. An example for results of magnetic measurements is given in Fig. 1. A unit implies $\times 10^{-4}$ for a value. The edge quadrupoles are subtracted by the analytical value, as it is discussed below. Measurements are performed for 20 current values, from $I = 1$ kA to $I = 13.5$ kA, which are visible with dots in Fig. 1 and further plots. The coil current is converted to the magnetic rigidity $B\rho$.

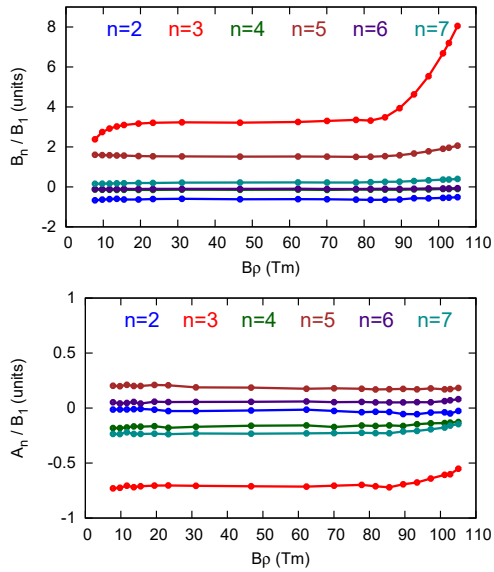

Figure 1: Normal (top plot) and skew (bottom plot) field error harmonics as functions of the coil current for one of the series SIS100 dipole magnets.

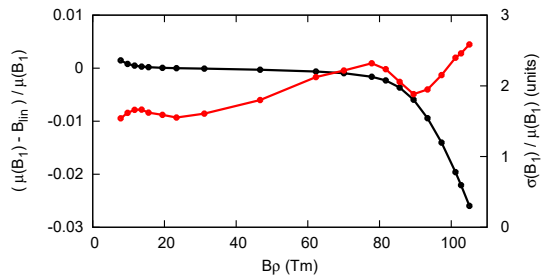

Figure 2: Deviation of the integrated bending field B_1 from a linear dependence Eq. (2) (black line, left axis). $\mu(B_1)$ implies average over the four series magnets. Red line, right axis: the standard deviation for the four series magnets.

The linear dependence of the bending B_1 magnetic field is given by

$$B_{\rm lin} = t_f \; I \;\; [\rm mT], \qquad (2)$$

where the coil current I is given in kA, $t_f = 147.84$, the effective magnet length is $L_{\rm eff}$ =3.061 m. The total bending power of the magnets is compared with the linear dependence in Fig. 2. Additionally, the sample standard deviation for these measurements is presented with the red line. This spread is below 3 units, which can easily be treated by the closed-orbit correction system. In the beam dynamics

ISBN: 978-3-95450-184-7 doi:10.18429/JACoW-IPAC2018-THPAF080

studies, up to 40 units have been considered within the safe operation.

The measurement coil is parallel to the magnetic axis, i.e. the coil follows the design beam trajectory. For the two side coil positions it means a non-perpendicular orientation of the coil with respect to the yoke. This produces an edge quadrupole, the related gradient strength can be estimated analytically,

$$kl = -\frac{\tan(\theta/2)}{\rho}. \quad (3)$$

A comparison of the edge gradient field B_2 for one of the series SIS100 dipole magnets with this analytical estimation is shown in Fig. 3. In the beam dynamics studies we subtract the measured quadrupole coefficient by this analytical value.

The sextupole component B_3 is the most prominent, see Fig. 1, and has a non-flat current behavior due to the iron properties. However, this dependence is well reproduced for different magnets, see Fig. 4. The rms spread of B_3 is below 1 units also at highest currents.

Numerical tools for analysis of the field measurements have been developed. Eventually, data from the main magnets will constitute the complete database. At the moment, data from four series dipole magnets are available. Results of a statistical analysis for this data is presented in Fig. 5. Measurements for $I = 2\,\mathrm{kA}$ ($B\rho = 15.6\,\mathrm{Tm}$) are considered here. The edge quadrupoles are subtracted by the analytical value, the error bars show the 2σ sample standard deviation.

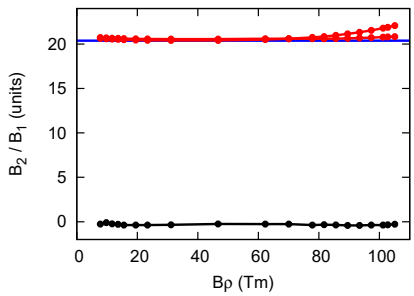

Figure 3: Quadrupole component from the field measurements for one of the series SIS100 dipole magnets. Red lines: for the two side coil positions; black line: for the magnet body. Blue line: estimation using Eq. (3).

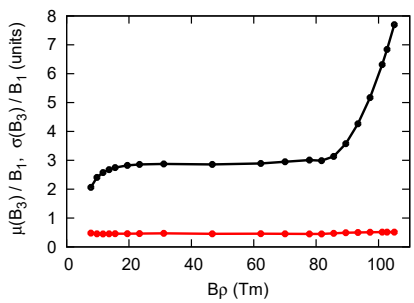

Figure 4: The total magnet sextupole component for the four series magnets. Black: the average $\mu(B_3)$, red: the standard deviation $\sigma(B_3)$.

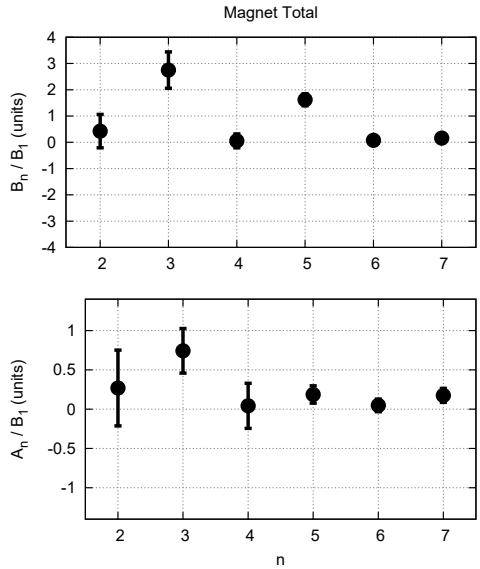

Figure 5: The overview of the systematic field error harmonics and the related standard deviations from the data of the four series magnets.

DYNAMIC APERTURE SIMULATIONS

The field error coefficients from Fig. 5 have been used to construct the model for the SIS100 dipole magnets. The average of the B_3, B_5, B_7 (allowed harmonics) have been taken as the systematic components, while the other systematic parts have been assumed zero. The sample standard deviations from Fig. 5 habe been used as the random components.

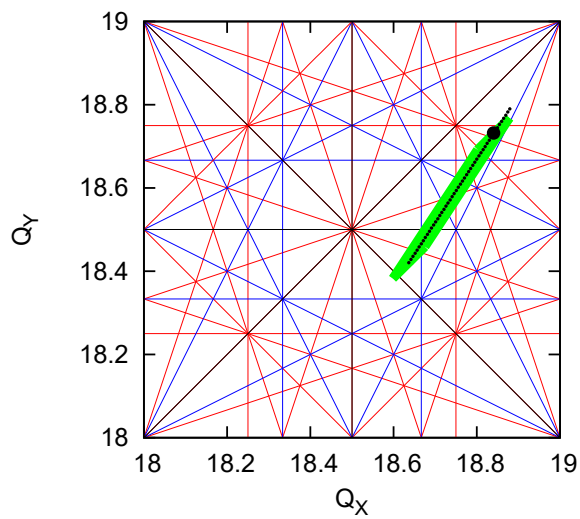

Figure 6: Tune diagram with the resonances up to fourth order. The black circle is a SIS100 tune, the green area schematically shows the single-particle tune spread.

ISBN: 978-3-95450-184-7 doi:10.18429/JACoW-IPAC2018-THPAF080

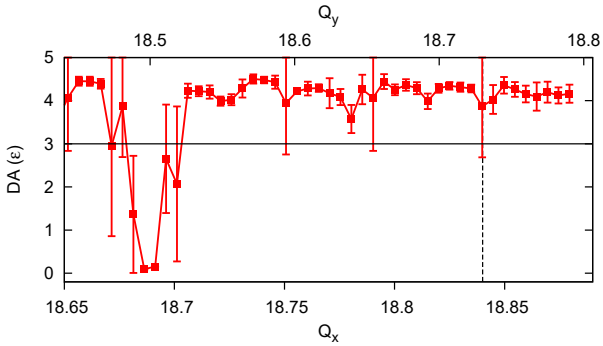

Figure 7: Results of the Dynamic Aperture scans in the transverse emittance units along the dot line from Fig. 6.

For the quadrupole magnets, the model based on the 3d simulations, equally to the studies [6, 7], has been used.

The Dynamics Aperture (DA) has been simulated using the MADX code [8]. Particle are tracked for not more than 10^3 turns (short-term DA), in a search for the minimal transverse emittance of stability [6, 7].

DA has been studied for the relevant tunes. The SIS100 machine tunes for the heavy-ion high-intensity operation with the fast extraction are $Q_x = 18.84, Q_y = 18.73$ [9]. The corresponding resonance diagram is shown in Fig. 6. Black lines are the second order (quadrupole) resonances, blue lines are the third order (sextupole) resonances, red lines are the fourth order (octupole) resonances. The main reason for the tune spread is space-charge (ΔQ_{sc} up to -0.3) [10] and the chromaticity, which is shown schematically in Fig. 6. Thus DA scans along the dot line are performed, see Fig. 7. For each random error seed, the tunes Q_x, Q_y and the chromaticities ξ_x, ξ_y are corrected to the set values using the main quadrupoles and the chromaticity sextupoles. DA values in Fig. 7 are given in the transverse emittance units, and are normalized by $\varepsilon = 35\,\text{mm mrad}$, which is the nominal total (2σ) horizontal emittance. The value 3ε (black line in Fig. 7) is considered as the safety criterion.

The closed orbit distortions are modeled using the following assumptions: the standard deviation of the total strength of the dipole magnets is $\sigma = 0.004\,B_1$, the transverse tilts of the dipole magnets are due to $\sigma_s = 1\,\text{mm}$ shifts, and the lateral shifts of the quadrupole magnets are $\sigma_s = 1\,\text{mm}$. These are the rms values of the applied Gaussian. The closed orbit distortions are corrected by the SIS100 steerers using the MICADO algorithm [8], the residual closed orbit distortion is $\Delta x_{\text{rms}} = 1.5\,\text{mm}$, $\Delta y_{\text{rms}} = 1\,\text{mm}$. A number of randomly generated close orbit distortions are considered, which results in the standard deviations of DA in Fig. 7.

In a conclusion, the field data from the four series dipole magnets demonstrate a sufficiently good field quality. The current dependencies of the field errors are flat (Fig. 1), with the exception of B_3, which is reproducible and gives a small random error (Fig. 4). The total bending power is also well reproducible and gives a small and easily correctable closed orbit distortion (Fig. 2). The overall field imperfections produce DA mostly above the safety criterion (Fig. 7).

The main challenge for SIS100 beam dynamics is the combined effect of space charge and the magnet field errors. Presently, production and measurements of the quadrupole magnets are in progress [11], which, together with further dipole magnet data, will provide the realistic SIS100 magnet system model. Development of simulations with space charge is in progress, with the aim to predict the beam losses for the different operation cycles, and the evolution of the beam quality (transverse size and distribution).

SLOW EXTRACTION

Simulation studies have been performed in order to estimate uncontrolled beam loss during slow extraction from SIS100. A special focus was on the influence of imperfections in the fields of dipole and quadrupole magnets. The standard technique for slow extraction from SIS100 is the so-called rf knock-out (KO) extraction, where the particles are extracted by excitation with a horizontal rf field. The settings for the unperturbed lattice are those presented in [12].

The strongest non-linear imperfections are the sextupole errors of the dipole magnets which depends on the excitation current of the magnets, see Fig. 4. The systematic contribution affects the horizontal chromaticity, whereas random variations alter the resonance excitation. The non-linear part of the particle motion is dominated by the chromaticity sextupoles rather than the resonance sextupoles leading to strong deviations from the linear theory such as bent separatrices, see Fig. 8. The black vertical line shows the position of the extraction septum.

The influence of random variations of non-linear errors is studied by determining particle losses for two scenarios. Initially, particle loss was calculated after introducing systematic and random magnet imperfections and optimizing the lattice in order to minimize particle losses at the electrostatic septum. In the next step, the lattice became optimized after introducing only systematic magnet errors and adding random variations afterwards. No significant increase of the particle losses were found which is a sign for the robustness of the simulations results against changes.

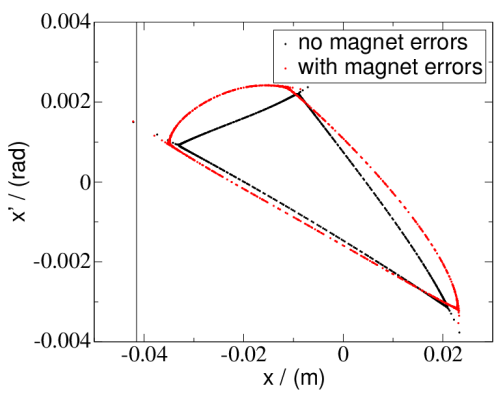

Figure 8: Horizontal stable phase space areas obtained with SIS100 lattices with for the highest rigidity and $\delta = 0$.

ISBN: 978-3-95450-184-7 doi:10.18429/JACoW-IPAC2018-THPAF080

REFERENCES

[1] P. Spiller *et al.*, in *Proc. IPAC2015*, Richmond, VA, USA, May 2015, DOI:10.18429/JACoW-IPAC2015-THPF015

[2] P. Spiller *et al.*, presented at IPAC2018, Vancouver, BC, Canada, April-May 2018, paper MOZGBF2, this conference

[3] E. S. Fischer *et al.*, in *Proc. IPAC2017*, Copenhagen, Denmark, May 2017, DOI:10.18429/JACoW-IPAC2017-WEOCB2

[4] C. Roux *et al.*, presented at IPAC2018, Vancouver, BC, Canada, April-May 2018, paper WEPML035, this conference

[5] F. Kaether *et al.*, in *Proc. IPAC2016*, Busan, Korea, May 2016, DOI:10.18429/JACoW-IPAC2016-TUPMB032

[6] V. Kornilov, O. Boine-Frankenheim, V. Kapin, in *Proc. IPAC2010*, Kyoto, Japan, May 2010, paper TUPD029, p. 1988

[7] C. Omet *et al.*, in *Proc. IPAC2015*, Richmond, VA, USA, May 2015, Richmond, VA, USA, May 2015, DOI:10.18429/JACoW-IPAC2015-WEPMA020

[8] MAD-X Code, http://cern.ch/madx

[9] G. Franchetti *et al.*, in *Proc. EPAC2006*, Edinburgh, Scotland, June 2006, paper THPCH005, p. 2793

[10] V. Kornilov, O. Boine-Frankenheim, in *Proc. IPAC2012*, New Orleans, Louisiana, USA, May 2012, paper WEPPR002, p. 2934

[11] E. Fischer *et al.*, presented at IPAC2018, Vancouver, BC, Canada, April-May 2018, paper WEPML030, this conference

[12] A. Saa-Hernandez *et al.*, in *Proc. IPAC2012*, New Orleans, Louisiana, USA, May 2012, paper TUPPC005, p. 1158